A new design method for retaining walls in clay

Ashraf S. Osman and Malcolm D. Bolton

Abstract: Geotechnical design engineers used to rely on arbitrary rules and definitions of "factor of safety" on peak soil strength in limit analysis calculations. They used elastic stiffness for deformation calculations, but the selection of equivalent linear elastic models was always arbitrary. Therefore, there is a need for a simple unified design method that addresses the real nature of serviceability and collapse limits in soils, which always show a nonlinear and sometimes brittle response. An approach to this method can be based on a new application of the theory of plasticity accompanied by the introduction of the concept of "mobilizable soil strength." This approach can satisfy both safety and serviceability and lead to simple design calculations within which all geotechnical design objectives can be achieved in a single step of calculation. The proposed method treats a stress path in an element, representative of some soil zone, as a curve of plastic soil strength mobilized as strains develop. Designers enter these strains into a plastic deformation mechanism to predict boundary displacements. The particular case of a cantilevered retaining wall supporting an excavation in clay is selected for a spectrum of soil conditions and wall flexibilities. The possible use of the mobilizable strength design (MSD) method in decision-making and design is explored and illustrated.

Key words: retaining wall, plasticity theory, design, finite element.

Résumé : Les ingénieurs géotechniciens avaient l'habitude de se fier dans leurs calculs d'analyse limite à des règles et définitions arbitraires du « coefficient de sécurité » basées sur la résistance de pic du sol. Ils utilisaient la rigidité élastique pour les calculs des déformations, mais la sélection de modèles équivalents élastiques linéaires était toujours arbitraire. En conséquence, on a besoin d'une méthode simple et unifiée de conception qui traite de la nature réelle de la praticabilité et des limites d'effondrement des sols, qui montre toujours une réponse non linéaire et parfois fragile. Une approche à cette méthode peut être basée sur une nouvelle application de la théorie de plasticité accompagnée de l'introduction du concept de « résistance mobilisable du sol ». Cette approche peut satisfaire tant la sécurité que la praticabilité, et peut conduire à des calculs simples de conception dans lesquels tous les objectifs de conception géotechnique peuvent être atteints au cours d'une étape unique de calcul. La méthode proposée considère un cheminement de contrainte dans un élément représentatif d'une certaine zone de sol, comme étant une courbe de résistance plastique du sol mobilisée à mesure que les déformations se développent. Les concepteurs entrent ces déformations dans un mécanisme de déformation plastique pour prédire les déplacements aux frontières. Le cas particulier d'un mur de soutènement en porte-à-faux retenant une paroi d'excavation dans l'argile a été choisi comme éventail des conditions des sols et de la flexibilités du mur. On explore et illustre l'utilisation possible de la méthode de calcul de la résistance mobilisable (MSD) pour la prise de décision et la conception.

Mots clés : mur de soutènement, théorie de plasticité, conception, éléments finis.

[Traduit par la Rédaction]

Introduction

Historically, plasticity theory has been used for calculating the distribution of lateral earth pressure, which is the central issue in the analysis of retaining structures. In this theory, a zone of soil is assumed to reach plastic equilibrium such that plastic collapse occurs. This plastic soil zone slips relative to the rest of the soil mass. The peak soil strength is assumed to be mobilized on the slip surface. The collapse load is then calculated and factors of safety are introduced to allow for uncertainties and to limit movements by ensuring that the stresses are far from their ultimate values. Different definitions of factors of safety are adopted in design codes and used in practice, however.

Received 29 April 2003. Accepted 5 December 2003. Published on the NRC Research Press Web site at http://cgj.nrc.ca on 29 June 2004.

A.S. Osman[1] and M.D. Bolton. Department of Engineering, Cambridge University, Trumpington Street, Cambridge CB2 1PZ, UK.

[1]Corresponding author (e-mail: aseko2@cam.ac.uk).

Code of practice (CP2)

Bolton (1993) illustrates the mixture of definitions of factor of safety in the *Code of practice for earth retaining structures* (CP2) (British Standards Institution 1994), which was first published in 1951. For a deep circular slip, a factor of safety of 1.25 is used and is defined as the restoring moment divided by the overturning moment. For embedded walls, the limiting passive resultant is reduced by a factor of 2, and the unfactored active value is used on the retained side. This was pointed out by Hubbard et al. (1984) as too conservative because, in certain design situations, a stronger and deeper wall is needed to achieve this arbitrary factor. It also creates an inconsistency, since the factor of safety can actually decrease with an increase of wall penetration in undrained conditions. Additionally, in drained conditions the

 doi: 10.1139/T04-003

Fig. 1. Earth pressure distribution at limiting conditions (after Padfield and Mair 1984). (*a*) Idealized distribution. (*b*) Simplified distribution.

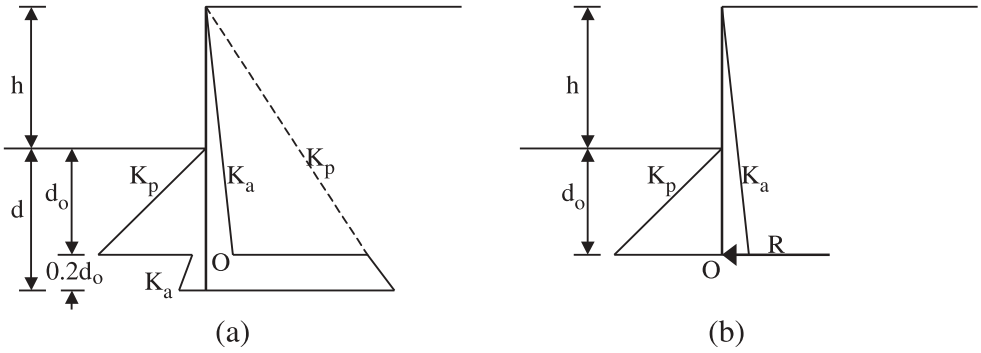

factor of safety has a finite value for zero height of retained material (Burland et al. 1981).

CIRIA report 104

Construction Industry Research and Information Association (CIRIA) report 104, which was published in 1984 (Padfield and Mair 1984), reviewed the current practice in applying safety factors. The stress distribution is simplified as shown in Fig. 1. The active and passive stresses below point O in Fig. 1 are replaced by the resultant force *R*. Moment equilibrium about point O is taken to determine the depth required for stability (d_0). This depth is then increased by 20% to account for that portion of wall over which the force *R* must be developed. The bending moments are calculated from the assumed pressure distribution (Padfield and Mair 1984).

CIRIA report 104 listed five methods of introducing a factor of safety:

(1) Increasing the embedded depth by a factor F_d — CIRIA report 104 accepted that this method could be used but advised that it should be checked against other methods. The main drawback of this method, however, is the assumption that the total stresses on both sides of the retaining wall below the depth just required to maintain equilibrium are equal and opposite (Powrie 1996).

(2) Reducing the soil strength parameters by a factor F_s — This method was adopted later on by the new British Standard BS 8002 (British Standards Institution 1994).

(3) Reducing the passive pressure coefficient by a factor F_p — This is based on the assumption that the in situ stresses are closer to those of the active state. A relatively small wall movement is needed to reach the active state, whereas an unacceptably large displacement is needed to reach the passive limit. In overconsolidated deposits, however, in situ stresses are closer to those of a passive state (Carder and Symons 1989; Garrett and Barnes 1984). Thus, the assumption of full active stresses may be inappropriate, as it could lead to the underprediction of lateral stresses (Symons 1983).

(4) Reducing the net available passive pressure by a factor F_r — In this method, which was developed by Burland et al. (1981), the net passive pressure under the excavation level is calculated from the net pressure coefficient ($K_p - K_a$) divided by a factor F_r (K_a and K_p are Rankine active and passive pressure coefficients, respectively). The embedded depth is then obtained by equating the moment calculated from the retained side to the moment of net pressure on the excavation side.

(5) Reducing the net passive pressure by a factor F_{np} — This method is used for propped walls. In this method, a net pressure diagram is plotted. The net passive pressure is divided by a factor F_{np}. The moment equilibrium about the prop is obtained by equating the net pressure moment on the passive side to the net pressure moment on the active side. This method may result in a safety factor F_{np} much smaller than the safety factor on the soil strength (F_s) (Burland et al. 1981). This method was not recommended by CIRIA report 104.

British Standard BS 8002

British Standard BS 8002 (British Standards Institution 1994) introduced a mobilization factor to prevent the stress levels in materials from reaching a point where the displacements become unacceptable. However, BS 8002 does not define any differences among mobilization factors required for permanent and temporary works (Puller and Lee 1996). Puller and Lee (1996) also showed that some inconsistencies arise in the practical application of the mobilization factors:

(1) BS 8002 suggests a mobilization factor that has the same value for any type of soil. The extent of strain needed to mobilize the peak strength varies from soil to soil, however. In loose soils, there is a less rapid mobilization of strength with the strain compared with dense soils. Therefore, the mobilization factors should be greater in loose soils than in dense soils.

(2) A constant value of the mobilization factor is suggested by BS 8002 irrespective of the depth. The deformed shape of the wall allows changes of strains with depth, however.

(3) Rigid gravity walls built from masonry may be relatively brittle. Thus, designers may wish to select smaller limiting strains, and therefore a larger mobilization factor.

Eurocode EC7

The design values in Eurocode EC7 (ECS 1997) are derived from characteristic values by applying partial factors. The characteristic values in Eurocodes are generally based on the notion that they will be selected so that only 5% of the sample values will be more unfavourable. Because of the lack of significant data in the case of geotechnical parameters, an alternative specification allows the designer simply

to select a cautious estimate for the characteristic value appropriate to occurrence of limit states. Having taken this judgment based on experience, the designer is instructed on the precise partial factor by which soil strengths, for example, are reduced. This rationale is based on a rather vague treatment of the probability of exceedence of peak strengths. It does not address the problem of excessive displacements (Simpson and Driscoll 1998).

Mobilizable strength design (MSD) method

In current design practice, there is a distinction between calculations for safety requirements and calculations for displacements. Plasticity theory is used in collapse calculations, whereas elasticity theory is used to predict displacements. The stresses under working conditions, however, are far from those obtained by plasticity theory, which predicts stresses at failure. The applications of elasticity theory are often complex and are based on an arbitrary equivalent modulus. Codes of practice do not deal with serviceability in any great depth (Simpson and Driscoll 1998).

Therefore, there is a need for a simple unified design approach that could relate successfully the real nature of serviceability and collapse limits to the soil behaviour. Bolton et al. (1989, 1990*a*, 1990*b*) proposed a new approach based on the theory of plasticity accompanied by the introduction of the concept of "mobilizable soil strength." The proposed design method treats a stress path in a representative soil zone as a curve of plastic soil strength mobilized as strains develop. Strains are entered into a simple plastic deformation mechanism to predict boundary displacements. Stresses are entered into simple equilibrium diagrams to demonstrate stability. Hence, the proposed mobilizable strength design (MSD) method might satisfy both safety and serviceability in a single step of calculation.

This paper focuses on the undrained shearing of clays to illustrate the MSD approach. Clays that remain undrained during construction must deform only in shear, and engineers use a shear stress τ rising towards an undrained shear strength c_u to define the loading of the material towards failure. To emphasise the concept that all shear stresses mobilize some shear strains, the symbol c_{mob} is used instead of τ and is referred to as the mobilized strength.

Figure 2 shows a kinematically admissible strain field that was derived from idealized soil behaviour in terms of uniformly deforming triangles, which are attached to the surrounding rigid zone through zero-extension lines. The verticals and horizontals represent frictionless displacement discontinuities. The triangles are free to slide along these surfaces. The simplified admissible field is compatible with a frictionless rigid wall rotating by a small angle $\delta\theta$ in undrained conditions (Bolton and Powrie 1988).

Since there is no volume change,

$$[1] \qquad \delta\varepsilon_{vol} = \delta\varepsilon_h + \delta\varepsilon_v = 0$$

where ε_{vol} is the volumetric strain; and ε_h and ε_v are the horizontal and vertical strains, respectively.

Using a minus sign as an indication of extension, the uniform increment in horizontal strain $\delta\varepsilon_h$ inside the triangle OAB can be calculated by the extension $h\delta\theta$ in AB:

Fig. 2. Kinematics admissible for undrained conditions.

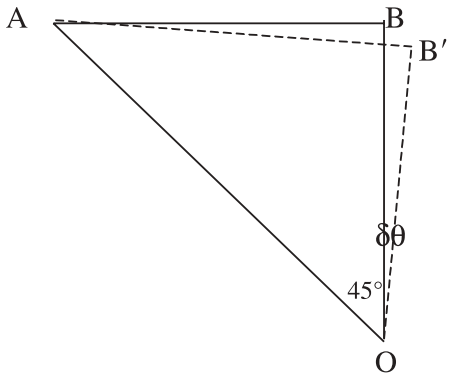

Fig. 3. Active and passive horizontal pressures mobilized in undrained conditions. σ_v, vertical stress.

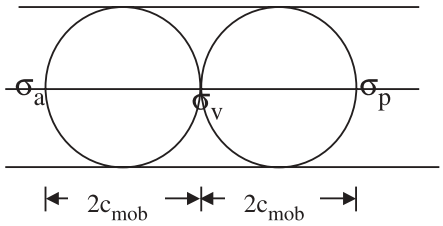

$$[2] \qquad \delta\varepsilon_h = \frac{-h\,\delta\theta}{h} = -\delta\theta$$

Substituting eq. [2] in eq. [1],

$$[3] \qquad \delta\varepsilon_v = \delta\varepsilon_{vol} - \delta\varepsilon_h = 0 - (-\delta\theta) = \delta\theta$$

The engineering shear strain increment $\delta\varepsilon_s$ is given by

$$[4] \qquad \delta\varepsilon_s = \delta\varepsilon_v - \delta\varepsilon_h$$

Thus

$$[5] \qquad \delta\varepsilon_s = \delta\theta - (-\delta\theta) = 2\delta\theta$$

Figure 3 shows an element mobilizing shear strength c_{mob}. The corresponding active pressure (σ_a) and passive pressure (σ_p) that can be mobilized at any depth z can be given by

$$[6] \qquad \sigma_a = \gamma z - 2c_{mob}$$

$$[7] \qquad \sigma_p = \gamma z + 2c_{mob}$$

where γ is the bulk unit weight of the soil.

Taking into account the possible lack of suction between the wall and the clay and the possible preexistence of vertical fissures that could open due to the development of tension, the depth of a dry tension crack (z_c) can be calculated as follows:

$$[8] \qquad \sigma_a = \gamma z_c - 2c_{mob} = 0$$

Then

$$[9] \qquad z_c = \frac{2c_{mob}}{\gamma}$$

Assuming that the wall is rotating about some point near its toe, the idealized stress distribution can be assumed as

Fig. 4. Lateral earth pressure distribution for an embedded cantilever wall in undrained conditions (K_0 = 1.0). *r*, height of the pivot point above the toe.

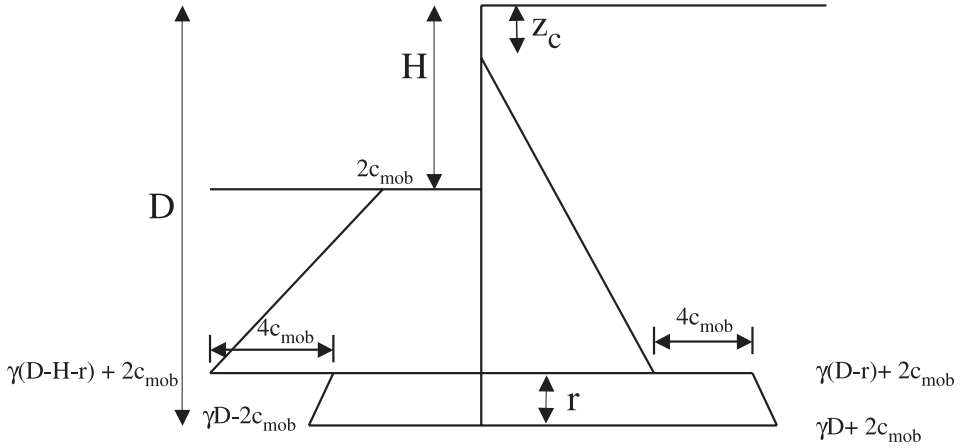

shown in Fig. 4, which must be in equilibrium. If the wall height *D*, excavation height *H*, and bulk unit weight of soil are known, the required strength and pivot position can be determined by solving the equations of force and moment equilibrium. Figure 5 shows the normalized undrained shear stress ($c_{mob}/\gamma D$) mobilized for different excavation height ratios (H/D) for an embedded cantilever retaining wall to achieve equilibrium. Figure 6 shows the ratio of the height of rotation point above the toe to the total height of the wall, for different relative excavation levels. The theoretical analysis shows that the maximum height of the pivot point is less than 2.5% of the total height of the wall. Although this simple mechanism is given for frictionless walls, Bolton et al. (1990*a*) concluded, from the investigation of data presented by Milligan and Bransby (1976), that it can be applied without significant error to rough walls.

The combination of the statical and kinematical approaches can offer a simple design method. The following assumptions can be made: active and passive zones in the two approaches correspond, and the mobilization of a uniform plastic strength c_{mob} is consistent with the development of a uniform plastic shear strain ε_{smob}. Thus, a stress-path test, in an element representative of some soil zone, can be treated as a curve of plastic soil strength mobilized as strains develop. Designers can enter these strains into the plastic deformation mechanism to predict boundary displacements. These assumptions represent the theoretical principles of the MSD method.

Figure 7 illustrates two possible procedures for using the MSD method in practice. In the first procedure (Fig. 7*a*), the maximum wall movement should not exceed a certain design value, which is suggested by the code or is selected according to the construction site situation. From the plastic deformation mechanism shown in Fig. 2, the designer can predict the mobilized strain. The strength mobilized can be obtained from the representative stress–strain curve. Figure 5 is then used to determine the excavation depth.

Another possible use of the MSD method is illustrated in Fig. 7*b*. The designer can check the acceptability of a particular depth of excavation. The corresponding wall displacement is then predicted using the MSD method. The excavated depth is acceptable if the calculated displacement is within the serviceability limit.

Fig. 5. Mobilized strength versus excavation depth.

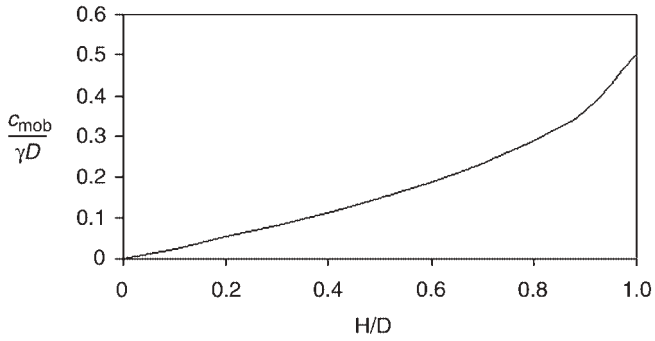

Fig. 6. Height of rotation point above the toe.

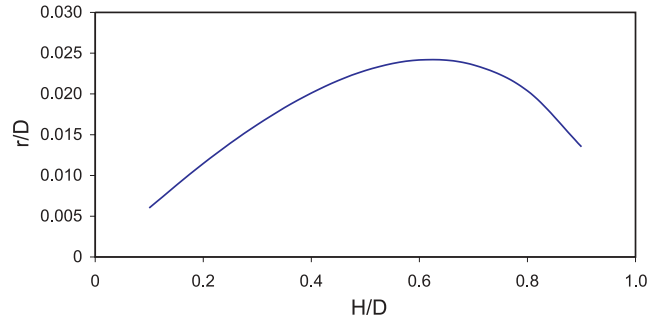

Finite element analysis

To examine the validity of the MSD method, its calculations were compared with finite element (FE) predictions. A series of two-dimensional plane strain FE analyses has been performed to predict the behaviour of cantilever retaining walls in the short term in which undrained conditions are assumed. Accordingly, excess pore pressure is not allowed to dissipate during the analysis. In all the analyses, it has been assumed that excavation of soil took place in front of a preformed cantilever retaining wall. Retaining walls in soft clays would certainly be propped or anchored near their crest. Accordingly, in the following demonstration, the clay is taken to be moderately or highly overconsolidated (Osman

Fig. 7. Possible design procedures.

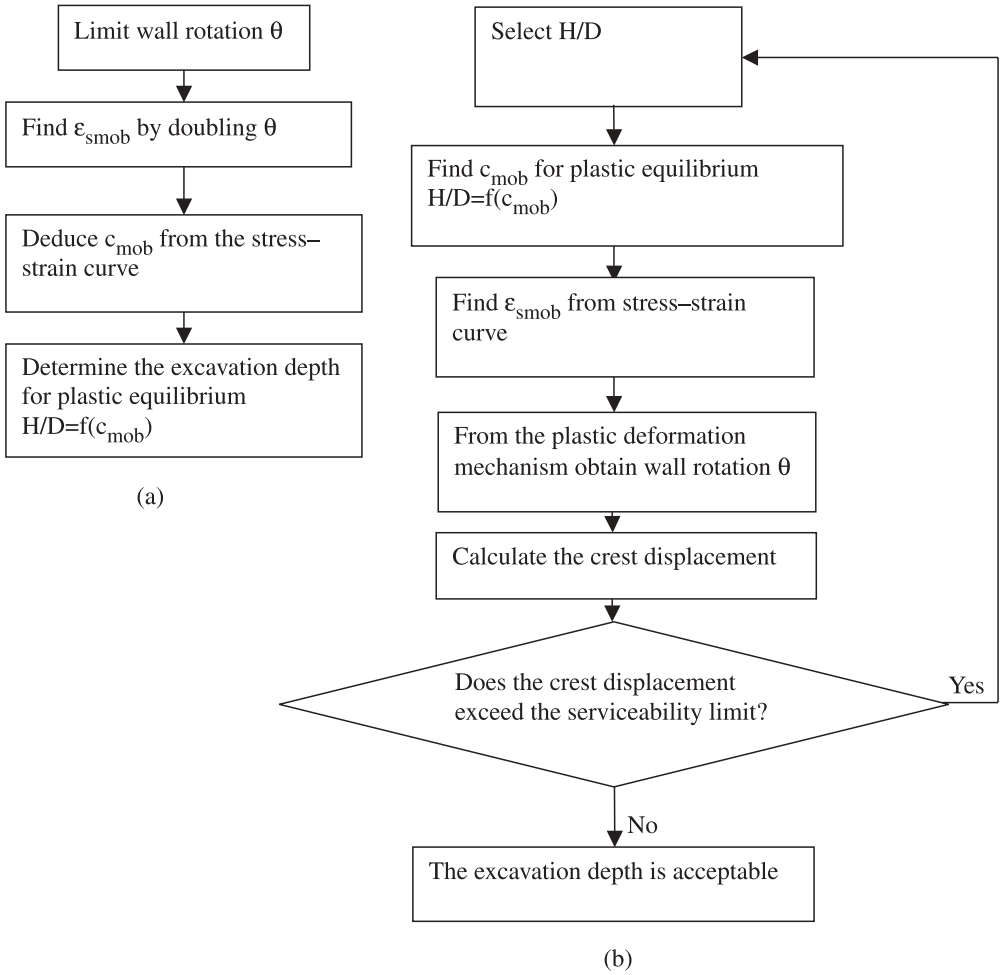

2002). The analyses were carried out using ABAQUS/STANDARD version 6.2 software.

The soil and the wall were modelled using eight-noded quadrilateral elements. Consolidation elements were used for the soil. The analyses modelled a half width of an excavation where the left-hand boundary of the mesh represents the line of symmetry at the centreline of the excavation. The mesh was sufficiently large to eliminate boundary effects so that the changes in stresses and displacements remote from the wall were negligible. Smaller elements were used near the wall where the changes of stresses and strains are significant. The bottom boundary was restrained from both horizontal and vertical movements, and the left- and right-hand boundaries were only restrained horizontally. Details of the FE mesh are shown in Fig. 8.

The wall was assumed to be made of reinforced concrete and to have properties equivalent to a typical diaphragm wall. The total height of the retaining wall is 20 m and its thickness is 1 m. The soil and the wall are assumed to stick together if the shear stress between the surfaces is less than a sliding shear stress of tan 26° times the normal effective stress between two contacting surfaces. The soil and the wall separate whenever the pressure reduces to zero or becomes negative (tension).

The water table is assumed to be initially at the ground surface. During the excavation no seepage flow is allowed to occur and the usual assumptions of undrained conditions analysis are taken to apply. In particular, negative pore pressures can be generated due to a reduction of total soil stresses following excavation in front of the wall.

Constitutive soil model

The stress–strain behaviour of the overconsolidated soil is highly nonlinear and the soil stiffness depends on the current state and the stress history (Atkinson et al. 1990; Jardine et al. 1984). The FE analyses conducted by Bolton and Sun (1991) for centrifuge tests of bridge abutments showed the importance of using a nonlinear elastoplastic model to predict the displacements and stresses on the abutment properly.

In the following FE simulation, the strain-dependent Modified Cam Clay (SDMCC) soil model (Dasari and Britto 1995; Dasari 1996) was used. This model can simulate the variation of stiffness with strain and the development of nonlinearity inside the yield surface, in addition to the effects of recent stress history. This model used Modified Cam Clay (Roscoe and Burland 1968) as a framework.

Figure 9 shows a typical variation in shear modulus in the SDMCC. At very small strain ($<10^{-5}$), the shear modulus (G) is at its maximum value (G_{max}) and is independent of the stiffness. It is a function of the overconsolidation ratio (OCR) and mean normal stress (p'):

Fig. 8. Finite element mesh.

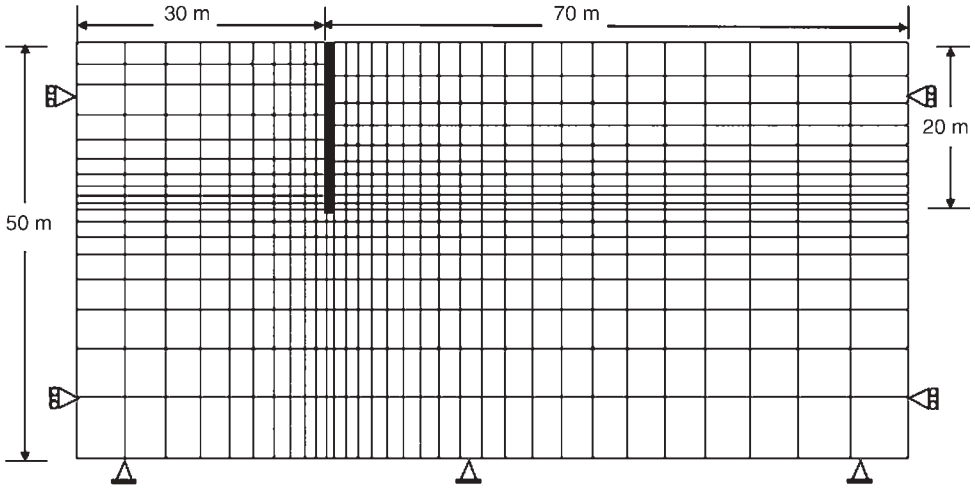

Fig. 9. Typical stiffness–strain relationship in the SDMCC model (after Dasari 1996). MCC, Modified Cam Clay; *A* and *B*, constants; ε_q, shear strain.

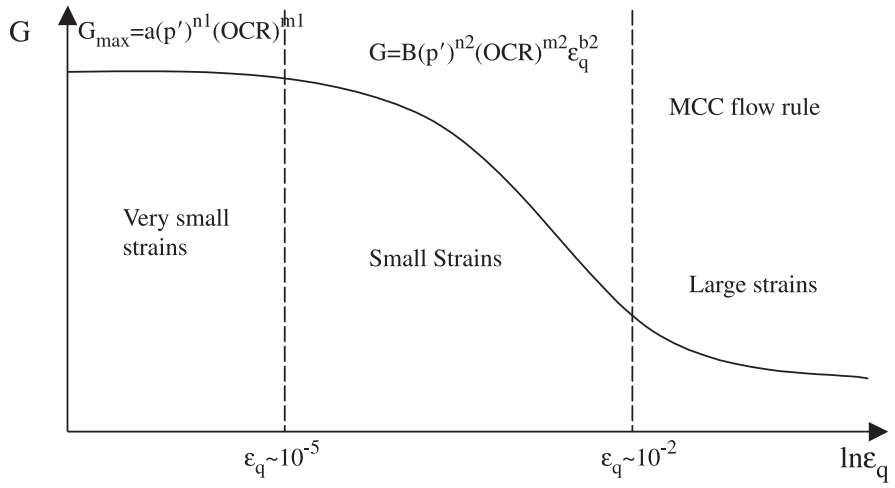

[10] $G_{max} = f(\text{OCR}, p')$

and is given by

[11] $G_{max} = A(p')^{n1}(\text{OCR})^{m1}$

where A, $n1$, and $m1$ are constants whose values should be selected using consistent units (kPa) for G_{max} and p'.

At small strains ($10^{-5} < \varepsilon_q < 10^{-2}$), the shear modulus depends on shear strains and also is a function of p' and OCR:

[12] $G = f(\varepsilon_q, \text{OCR}, p')$

and is given by

[13] $G = B(p')^{n2}(\text{OCR})^{m2}\varepsilon_q^{b2}$

where B, $n2$, $m2$, and $b2$ are constants.

At large strains the Modified Cam Clay (MCC) flow rules govern the stress–strain relation. Unloading–reloading loops are modelled by Masing's rule (Masing 1926). The stiffness–strain curve during the subsequent unloading and reloading is given by

[14] $G = B(p')^{n2}(\text{OCR})^{m}\left(\frac{\varepsilon_r - \varepsilon_q}{2}\right)^{b2}$

where ε_r is the reference strain corresponding to the point of the last reversal, and ε_q is the current deviatoric strain. Bulk modulus (K_{max}) is a function of p', OCR, and ε_v:

[15] $K_{max} = C(p')^{n3}(\text{OCR})^{m3}$

[16] $K = C(p')^{n4}(\text{OCR})^{m4}\varepsilon_v^{b4}$

where C, $n3$, $m3$, D, $n4$, $m4$, and $b4$ are constants. The derivation of the various parameters was explained by Bolton et al. (1994) and Dasari (1996). Table 1 lists the soil parameters used in the analysis.

In situ stress conditions

The stress history of the soil was assumed to comprise one-dimensional consolidation followed by the removal of effective overburden pressure of 1100 kPa to create a heavily overconsolidated clay.

Table 1. Parameters for the strain-dependent Modified Cam Clay (SDMCC) soil model.

Unit weight and permeability	
Unit weight of water, γ_w (kN/m^3)	10
Bulk unit weight of soil, γ (kN/m^3)	20
Permeability in vertical direction, k_v (m/s)	10^{-8}
Permeability in horizontal direction, k_h (m/s)	10^{-8}
Soil parameters for Modified Cam Clay soil model	
Slope of one-dimensional compression line in v – ln p' space, λ	0.161
Slope of unload–reload line in v – ln p' space, κ	0.062
Slope of critical state line in q–p' space, M	0.89
Void ratio on critical state line at p' = 1 kPa, e_{cs}	1.45
Poisson's ratio, ν	0.2
Parameters for shear modulus	
A	319
$n1$	1.0
$m1$	0.2
B	5.6
$n2$	1.0
$m2$	0.2
$b2$	–0.351
Parameters for bulk modulus	
C	304
$n3$	1.0
$m3$	0.2
D	1.147
$n4$	1.0
$m4$	0.2
$b4$	–0.488

It is well known that the behaviour of soil is strongly influenced by its stress history. Wall installation imposes certain changes in stress, so it defines the stress history prior to excavation. As a result, it affects soil response during the excavation. In situ lateral stresses in the vicinity of a diaphragm wall tend to reduce as a result of wall construction (Powrie et al. 1998; Symons and Carder 1992; De Moor 1994).

The main analyses in this study were accordingly carried out with an initial lateral earth pressure coefficient at rest (K_0) equal to unity following the technique initiated by Powrie and Li (1991) to model installation effects. This approach is consistent with field measurements reported by Tedd et al. (1984) which showed that K_0 reduced to unity from an initial value of 1.5 as an effect of wall installation.

Comparison between MSD and FE

Simulation of soil behaviour in the MSD method

It is well known that a complete solution for any deformable body in geotechnical engineering requires satisfaction of three components: equilibrium, compatibility, and material behaviour. In the MSD method, the equilibrium and compatibility conditions were satisfied through the statically and kinematically admissible mechanisms, which were illustrated earlier. The following framework was adopted for material properties:

(1) The soil is homogenous.
(2) The displacements are controlled by the average soil stiffness in the zone of the deformation.
(3) A representative stress–strain curve for soil at mid-depth of the retaining wall can be used to deduce the average shear strain, which is mobilized in the MSD calculations.
(4) FE simulation of an undrained triaxial test was used to plot the representative stress–strain curve. The initial conditions of the simulated triaxial sample correspond to in situ conditions of the representative soil element prior to the excavation. This FE simulation would be replaced in practice by the triaxial data of an undisturbed sample.

Case 1: a retaining wall supporting a highly overconsolidated clay with K_0 = 1.0

In this case, a retaining wall was assumed to support an excavation in overconsolidated clay. The justification of K_0 = 1 in heavily overconsolidated soil is that the construction of an in situ concrete wall would cause K_0 to drop to unity (Powrie 1985). The wall was 20 m high and 1 m thick. The wall was assumed elastic and impermeable with a Young's modulus (E) of 2.8×10^7 kPa and Poisson's ratio (ν) of 0.15. Therefore, the bending stiffness (EI) is 2.33×10^6 kN·m^2/m, which is typical for in situ concrete retaining walls (Long 2001). The unit weight of the wall was taken to be 22 kN/m^3. The profile of in situ undrained strength of the clay is shown in Fig. 10.

Fig. 10. Undrained strength (c_u) profile (case 1).

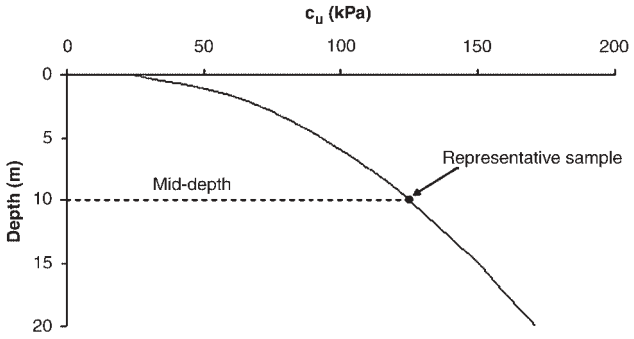

Fig. 11. Representative stress (q) – strain (ε_q) curve for case 1.

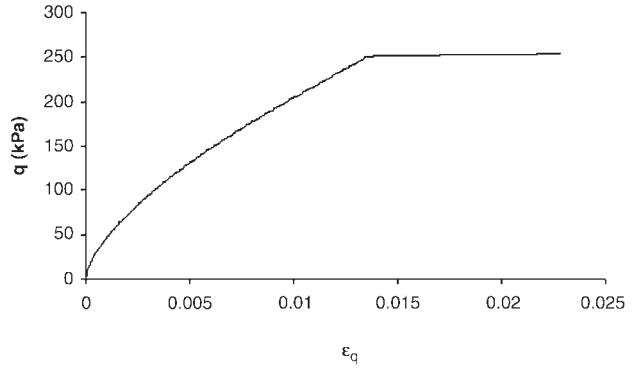

The following example illustrates the MSD method calculations. Suppose a rigid wall of height D 20 m supports a retained height H of 5 m, then $H/D = 5/20 = 0.25$. The bulk unit weight of the soil γ is 20 kN/m^3. The mobilized shear strength from Fig. 5, for $H/D = 0.25$ and bulk unit weight of soil (γ) of 20 kN/m^3, is $c_{mob}/\gamma D = 0.0675$, giving a mobilized shear stress (c_{mob}) of $0.0675 \times 20 \times 20 = 27$ kPa.

Since the deviatoric stress mobilized (q_{mob}) is twice the shear strength, then $q_{mob} = 2c_{mob} = 2 \times 27 = 54$ kPa. From the stress–strain curve plotted in Fig. 11, the corresponding triaxial shear strain (ε_q) is 0.00125. The engineering shear strain (ε_{smob}), which has to be mobilized, is equal to 1.5 times the triaxial shear strain ε_q, and thus $\varepsilon_{smob} = 1.5\varepsilon_q = 1.5 \times 0.00125 = 0.00188$. From the plastic deformation mechanism (eq. [5]), therefore, $2\delta\theta = 0.00188$ and $\delta\theta = 0.00188/2 = 0.00094$.

The height of the pivot point above the toe (r), normalized by the overall height (D), for various excavation ratios is plotted in Fig. 6. For $H/D = 0.25$, $r/D = 0.0115$. Thus $r = 0.0115 \times 20 = 0.23$ m. The height of the wall above the rotation point (L) (Fig. 9) is given by $L = D - r = 20 - 0.23 = 19.77$ m. The displacement at the top of the wall (Δ) is therefore given by $\Delta = \delta\theta L = 0.00094 \times 19.77 = 0.019$ m = 19 mm.

Table 2 compares the MSD predictions of lateral movements at the top of the wall with FE calculations as the excavation proceeds to 10 m depth. Figure 12 shows the close match between the total lateral horizontal stresses predicted by the FE method and those by the MSD method.

Figure 13 shows that the 45° deformable wedge deformations can be accepted as a simplified serviceability mechanism for the wall and its neighbouring soil zones. If the focus of concern for soil movements lies outside the simple 45° wedge, it is possible that a simplified extension field of equilibrium stresses could be derived, from which far-field strains might be estimated, but this is beyond the scope of the current paper.

Fig. 12. Lateral stress distribution (case 1): (*a*) 5 m excavation, (*b*) 8 m excavation, (*c*) 10 m excavation.

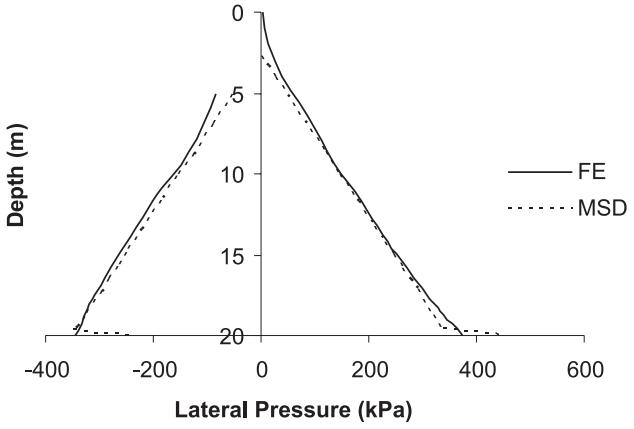

(a)

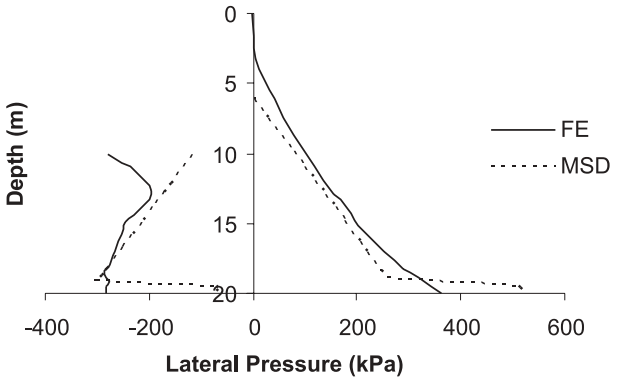

(b)

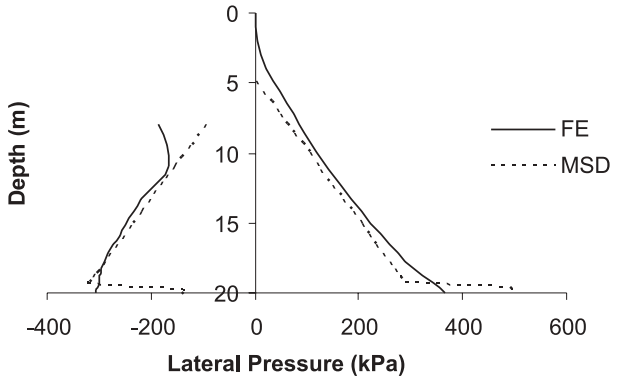

(c)

Table 2. Mobilizable strength design (MSD) calculations of displacements (K = 1.0).

	MSD method								FE analysis
Depth of excavation (m)	H/D	$c_{mob}/\gamma D$	c_{mob} (kPa)	q_{mob} (kPa)	ε_q	ε_{smob}	$\delta\theta$	Δ_{MSD} (mm)	Δ_{FE} (mm)
3	0.15	0.045	18	36	0.00067	0.00100	0.0005	10	16
5	0.25	0.075	27	54	0.00125	0.00188	0.0009	19	31
8	0.40	0.120	48	96	0.00308	0.00462	0.0023	45	62
10	0.50	0.150	60	120	0.00438	0.00657	0.0033	64	90

Fig. 13. Vectors of the displacements (5 m excavation depth).

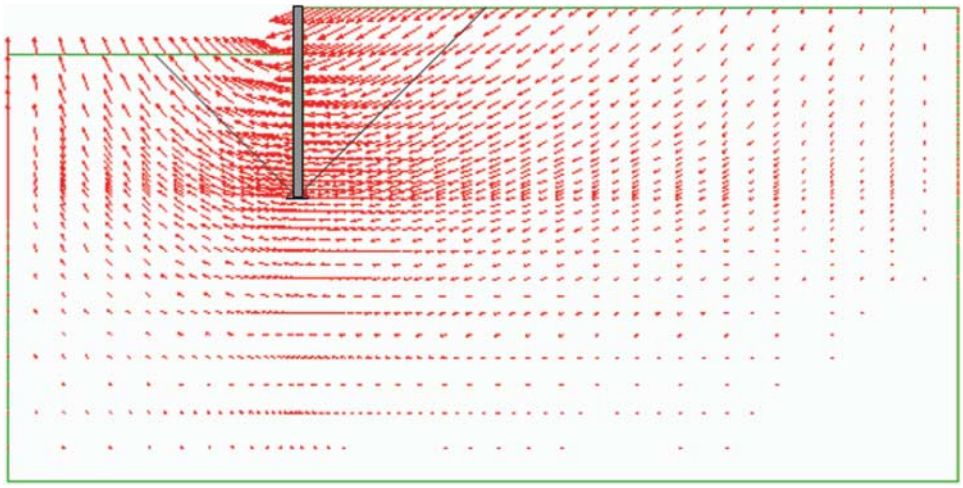

The MSD method gives a reasonable approximation of both the wall movement and the lateral stress distribution, compared with the FE results. The FE results show some reduction in stresses towards the toe of the wall on the excavation side and a corresponding increase on the retained side at the same location. This agrees with the assumption that retaining walls rotate about some point near the toe. The location of the pivot point predicted by the MSD method is similar to that calculated by the FE method.

The FE analysis shows only shallow tension cracks compared with the MSD analysis (Fig. 12). Two centrifuge results reported by Bolton and Powrie (1987) showed that in the case of walls of deeper penetration ratio, the soil displacements are compatible with the movements of rigid walls. The soil and the wall remained in contact and tension cracks did not develop. The excavation depth at prototype scale for the two tests was 10 m and the wall height was 25 and 30 m in the first and second tests, respectively. Bolton and Powrie also reported two other centrifuge tests in which unpropped walls had shallow penetration depths of 10 and 5 m and the total heights of the walls were 20 and 15 m, respectively. In these tests, fluid-filled tension cracks developed. Equilibrium of the wall in undrained conditions depends on the generation of large negative pore pressures near the wall and transmission of tensile soil stress at the soil–wall interface on the active side (Bolton and Powrie 1987). With a shallow penetration depth, the wall rotation is relatively large and the soil–wall interface will be incapable of transmitting the corresponding tension, leading to the development of cracks. Crack development depends on the displacements and the stiffness of both the soil and the wall, which are not taken into account in the MSD simple stress field.

Figure 14 shows that MSD method can give reasonable predictions of bending moments. The MSD method calculates bending moments from the assumed stress distribution, however, regardless of the flexibility of the wall. The magnitude of the maximum bending moment that the wall will attract depends on the stiffness of the wall (Potts and Fourie 1985). Figure 15 compares bending moments calculated by the FE method for a variety of wall stiffnesses. Although very stiff walls can attract larger bending moments, a ductile retaining wall designed to resist MSD earth pressure cannot collapse. If it is so stiff that it would develop bending moments in excess of the MSD values, plastic deformations will cause some extra wall displacements that relieve the earth pressures and reduce the bending moments. If the retaining walls are designed to be ductile at yield, as with underreinforced concrete sections, it is not necessary to design them as stiff elastic members to carry worst credible bending moments. Figure 16 illustrates the behaviour of two retaining walls. The walls are very stiff (EI = 1.43×10^8 kN·m^2/m). The first wall was modelled as an elastic material and the second as an elastic–plastic material designed to resist only MSD bending moments. Figure 16*b* shows that yielding only causes about 20% more displacement. In this

Fig. 14. Bending moment distribution (case 1): (*a*) 5 m excavation, (*b*) 8 m excavation, (*c*) 10 m excavation.

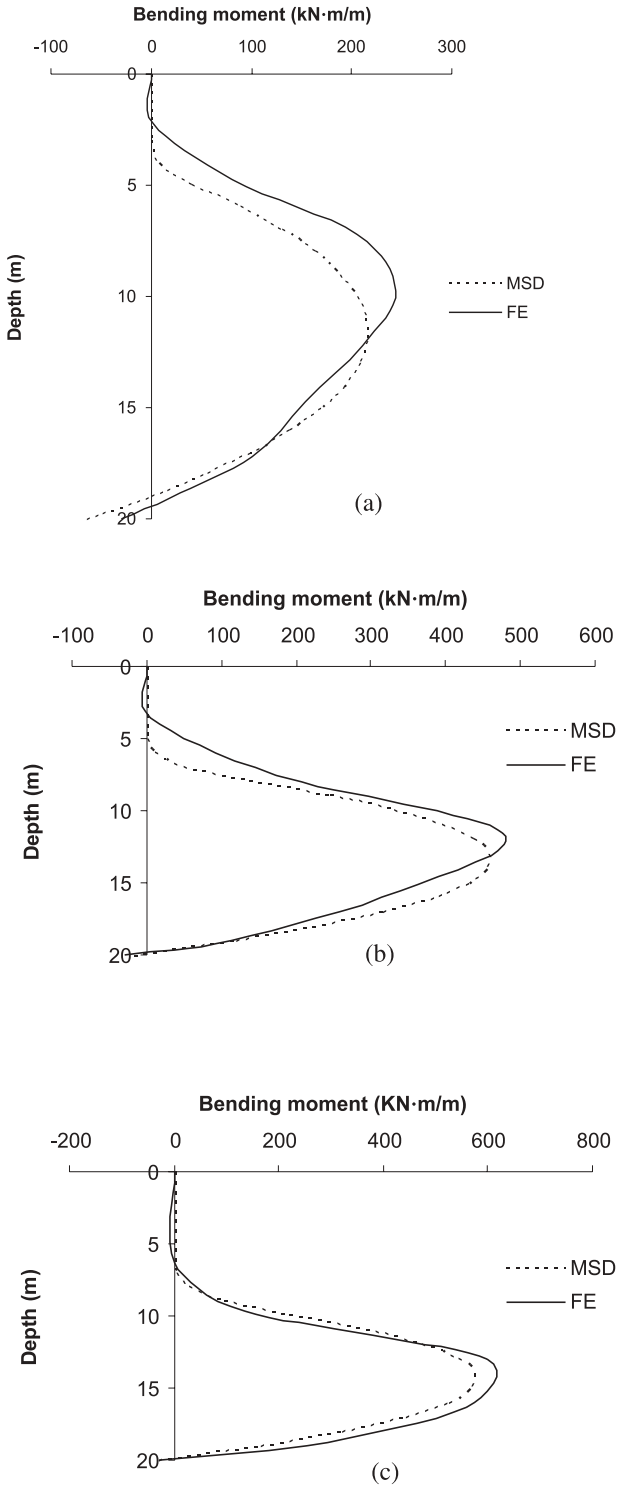

Fig. 15. Effect of wall flexibility on bending moments for 10 m excavation.

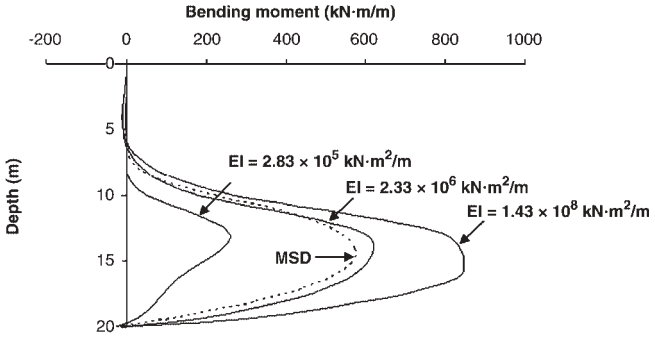

Fig. 16. Effect of modelling retaining walls (very stiff wall, EI = 1.43×10^8 kN·m^2/m).

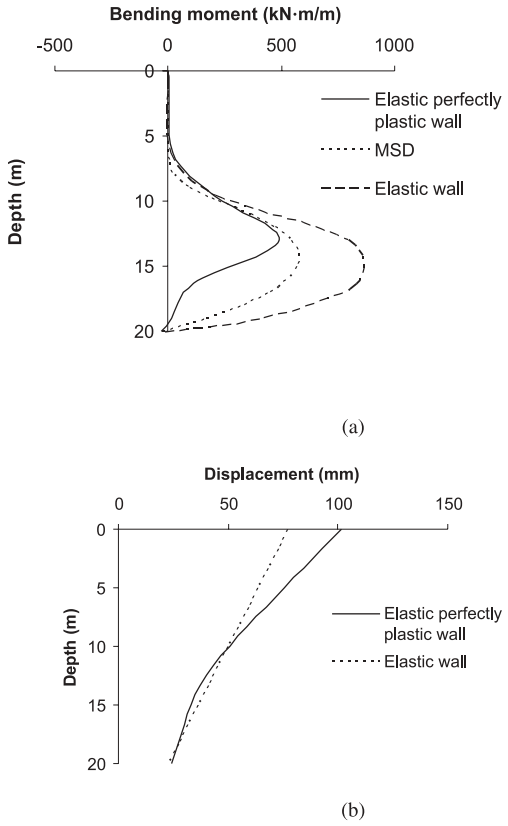

Fig. 17. Representative stress–strain curve for case 2.

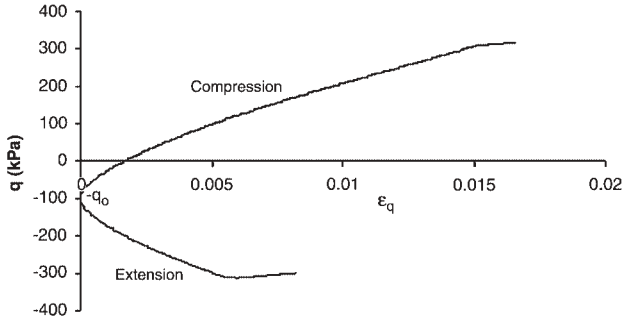

Table 3. Mobilizable strength design (MSD) calculations of displacements (K = 2.0).

		MSD method									FE analysis
Depth of excavation (m)	H/D	$\Delta c_{mob}/\gamma D$	Δc_{mob} (kPa)	Δq_{mob} (kPa)	Active q_{mob} (kPa)	Passive q_{mob} (kPa)	ε_q	ε_{smob}	$\delta\theta$	Δ_{MSD} (mm)	Δ_{FE} (mm)
3	0.15	0.045	18	36	–64	–136	0.0003	0.0005	0.0003	6	14
5	0.25	0.075	30	60	–40	–160	0.0008	0.0013	0.0006	13	27
8	0.40	0.135	54	108	8	–208	0.0020	0.0030	0.0015	30	55
10	0.50	0.185	76	152	52	–252	0.0034	0.0051	0.0026	51	84

Fig. 18. Change in mobilized strength versus excavation depth.

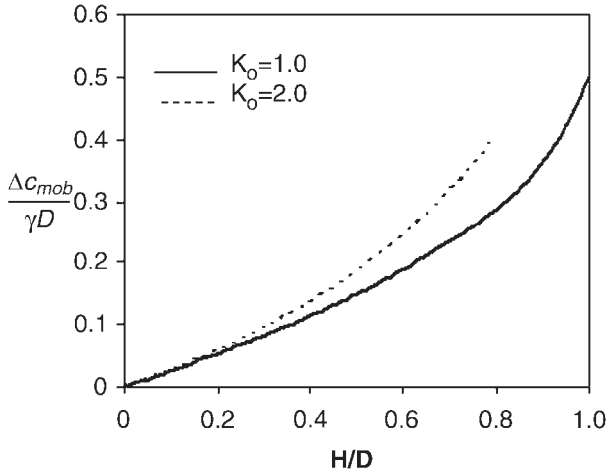

Fig. 19. Height of rotation point above the toe (K_0 = 2).

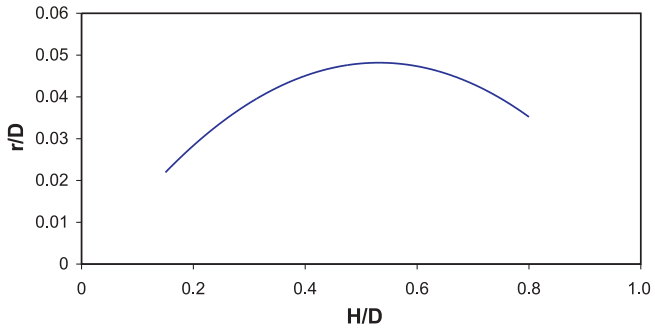

case, designers will be relying on the durability of reinforced concrete where small cracks have occurred and where the steel is at yield.

Case 2: a rigid wall supporting highly overconsolidated clay with K_0 = 2.0

In this case, the validity of MSD assumptions was examined for a typical concrete wall supporting highly overconsolidated London clay, which somehow retains a K_0 value of 2.0.

The permissible stress field shown in Fig. 4 is inappropriate if the preexcavation earth pressure coefficient is not equal to unity, because some soil strength is being mobilized on both sides of the wall before any wall movement takes place. An alternative stress distribution can be derived as follows. Consider a soil element at depth z below the ground surface (assuming the water level is at the ground surface). The initial effective horizontal stress (σ'_h) can be approximated by

$$[17] \quad \sigma'_h = K_0(\gamma - \gamma_w)\, z$$

where γ is the bulk unit weight of the soil, and γ_w is the unit weight of water. Thus, the total lateral pressure (σ_h) exerted on a frictionless rigid wall installed in the ground, prior to excavation, is given by

$$[18] \quad \sigma_h = K_0(\gamma - \gamma_w)\, z + \gamma_w z$$

This equation can be rewritten in the form

$$[19] \quad \sigma_h = \gamma z + (K_0 - 1)(\gamma - \gamma_w)\, z$$

The vertical stress is given by

$$[20] \quad \sigma_v = \gamma z$$

Therefore, prior to excavation, the soil with $K_0 \neq 1.0$ has an initially mobilized deviator stress (q_o) given by

$$[21] \quad q_o = (K_0 - 1)(\gamma - \gamma_w)\, z$$

The active pressure (σ_a) and passive pressure (σ_p) at any depth z can then be given by

$$[22] \quad \sigma_a = \gamma z + q_o - 2\Delta c_{mob}$$

and

$$[23] \quad \sigma_p = \gamma z_p + q_o + 2\Delta c_{mob}$$

where Δc_{mob} is the change of mobilized strength induced by wall movement, z is the depth measured from the ground level, and z_p is measured from the excavation level. The value q_o merely increases all the stresses and reduces the depth of tension. The depth of a dry tension crack (z_c) can be calculated by

$$[24] \quad z_c = \frac{2\Delta c_{mob}}{\gamma + (K_0 - 1)(\gamma - \gamma_w)}$$

In this case study, the constitutive model used in FE analysis happened to give an identical change of stress versus change of strain for compression and extension stress paths in the nonlinear elastic zone. This was because of the adoption of isotropy and the simplification of the stress history during wall construction. Accordingly, there is an initially unique relationship between change of mobilized strength Δc_{mob} and wall rotation, provided that the soil remains elastic (Fig. 17). The MSD calculation procedure can be refined

Fig. 20. Lateral stress distribution (case 2): (*a*) 5 m excavation, (*b*) 8 m excavation, (*c*) 10 m excavation.

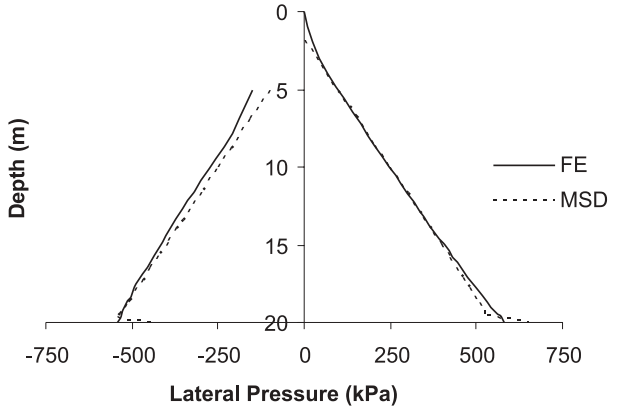

(a)

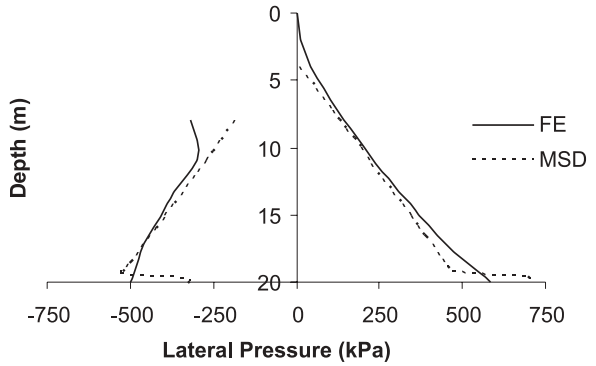

(b)

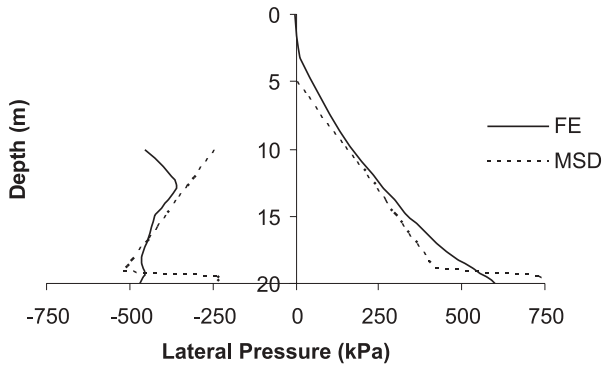

(c)

Fig. 21. Bending moment distribution (case 2): (*a*) 5 m excavation, (*b*) 8 m excavation, (*c*) 10 m excavation.

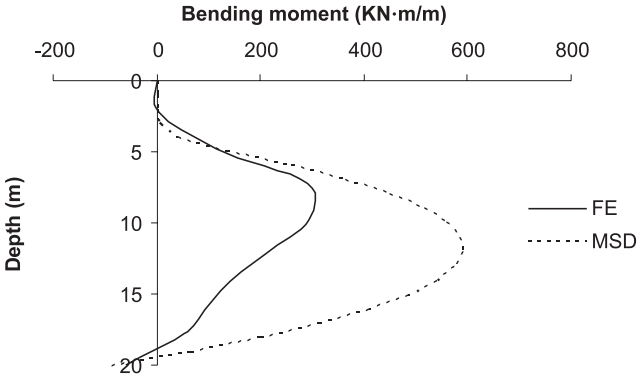

(a)

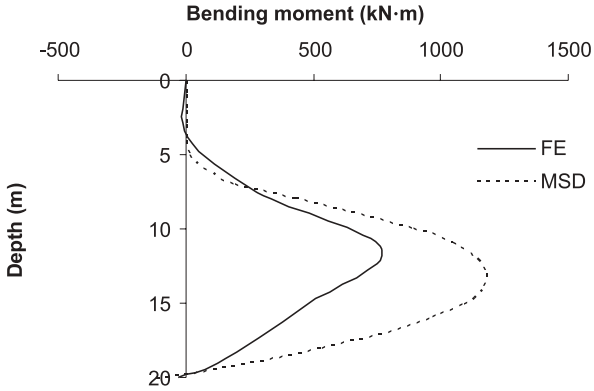

(b)

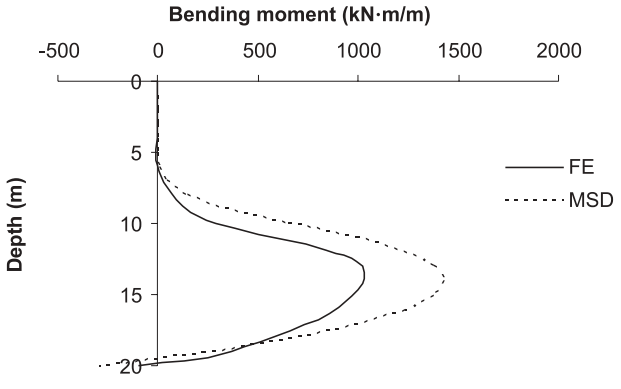

(c)

Fig. 22. Maximum shear modulus profile.

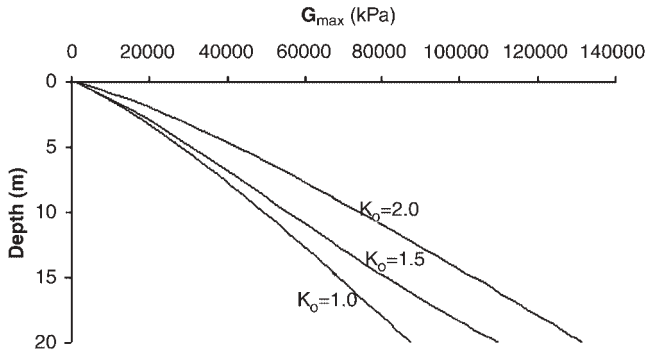

to take into account the differences between stress–strain curves in the active and passive zones whether due to soil stress history or anisotropy as follows:

(1) Select the allowable displacement for the retaining wall.
(2) Find the corresponding mobilized strain applicable to all deformation zones.
(3) Determine the active and passive strengths mobilized from compression and extension triaxial tests, respectively. In these tests the stress paths followed during wall installation and during excavation of the soil in front of the wall should be taken into account (Powrie et al. 1998). The corresponding excavation depth can then be determined by solving the equilibrium equations.

Figure 18 provides a solution for the normalized change of the mobilized strength ($\Delta c_{mob}/\gamma D$) in the two cases where $K_0 = 2.0$ and $K_0 = 1.0$, for the particular condition $\gamma/\gamma_w = 2$, the initial water table at the ground surface, and assuming that Δc_{mob} remains the same for both sides of the wall. The MSD solution shows that the magnitude of the change in mobilized strength in the case of walls of deeper penetration is not much affected by the value of K_0. The effect of K_0 on the mobilized strength increases with the increase of excavation. At $H/D = 0.4$, the change in mobilized shear strength is about 18% larger in the $K_0 = 2.0$ case than in the $K_0 = 1.0$ case. The pivot point calculated on this assumption is about 5% of the total wall height above the toe in the $K_0 = 2.0$ case (Fig. 19).

Table 3 shows a comparison of the predicted displacements between FE and MSD for $K_0 = 2.0$. In the MSD calculations the representative stress–strain curve of Fig. 17 was used. Figure 20 compares the lateral stress distributions. The MSD bending moment predictions are shown in Fig. 21 to be conservative with respect to FE analysis, but not excessively so. The new approach of allowing for an offset in initial deviatoric stress due to K_0 effects is shown to be successful.

Effects of wall flexibility and K_0

The impact of the various parameters that influence wall movements in the short term was studied. The displacements of the crest of the wall calculated by the MSD method (Δ_{MSD}) are normalized by the FE displacements (Δ_{FE}) and are related to wall flexibility for different in situ lateral earth pressure coefficients (K_0), different shapes of soil stress–strain curve, and different excavation ratios, defined as the excavated depth divided by the overall height of the wall.

Fig. 23. Comparison of crest displacements between FE calculations and MSD predictions for different K_0 values: (*a*) H/D = 0.25, (*b*) H/D = 0.40, (*c*) H/D = 0.50.

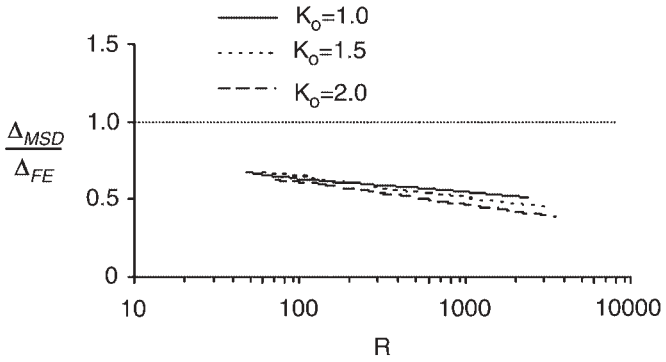

(a)

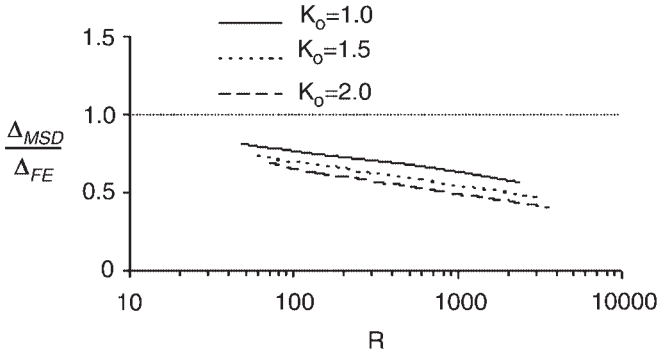

(b)

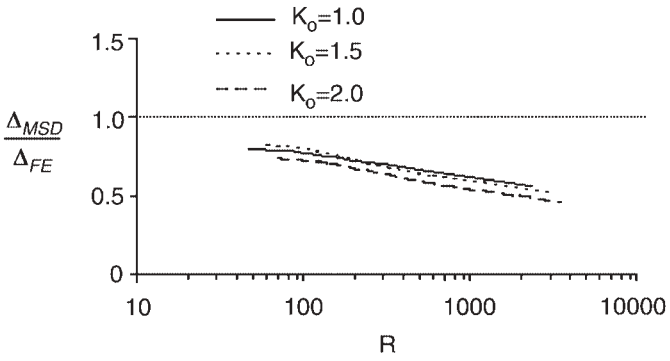

(c)

The wall flexibility can be characterized by the nondimensional group (R), which was introduced by Rowe (1955). R is defined as the relative soil–structure stiffness and is given by

$$[25] \quad R = \frac{mH^4}{EI}$$

Fig. 24. Different shapes of stress–strain curve (K_0 = 1.0).

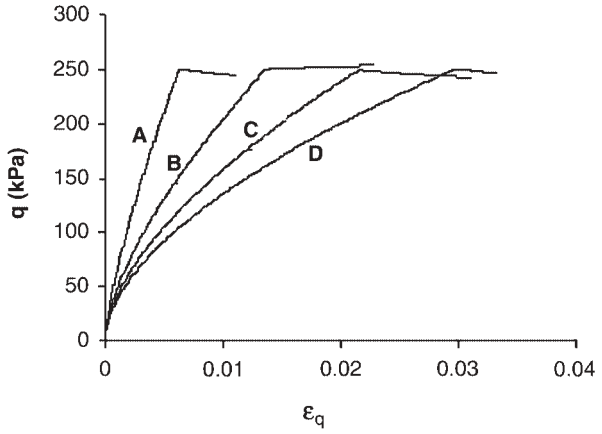

Table 4. Shear modulus parameters for the SDMCC constitutive soil model for different stress–strain curves.

Curve	*A*	*n*1	*m*1	*B*	*n*2	*m*2	*b*2
A	319	1.0	0.2	17.94	1.0	0.2	–0.250
B	319	1.0	0.2	5.60	1.0	0.2	–0.351
C	319	1.0	0.2	3.19	1.0	0.2	–0.400
D	319	1.0	0.2	2.26	1.0	0.2	–0.430

where H is the height of the wall, and EI is the bending stiffness per unit width. The parameter m can be defined as the rate of change of the shear modulus with depth (Powrie and Li 1991). In this case, it may be acceptable to calculate a representative m by fitting the best straight line through the origin of the plot of the maximum shear modulus (G_{max}) versus depth (Fig. 22).

Figure 23 summarizes the relation between MSD predictions and FE calculations of the displacements for various K_0 values. The ratio Δ_{MSC}/Δ_{FE} does not seem to be affected much by K_0 values. Figure 24 shows different representative shapes of stress–strain curve for samples extracted from the same in situ conditions with K_0 = 1.0. Curve B represents the same stress–strain curve of Fig. 11 that was used in the simulation shown in Fig. 23. Curve A exhibits smaller strain to failure, whereas curves C and D show larger strain to failure, but all share the same maximum shear modulus (G_{max}). The soil parameters used in the simulation are given in Table 4. Figure 25 compares FE calculations and MSD predictions for the different stress–strain curves.

Evidently, MSD predictions are most accurate when the soil stiffness deteriorates most markedly. It must be inferred from Fig. 25 that the underprediction of displacement ($\Delta_{MSD}/\Delta_{FE} < 1$) of stiff walls ($R \approx 50$) for all K_0 values, shown in Fig. 23, was largely due to the shape B of the stress–strain curve used in the calculations. For the whole range of wall flexibilities, initial earth pressure coefficients, and shapes of stress–strain curves studied here, the MSD predictions underestimate FE analyses, but generally by a factor of not more than 2.

If Figs. 23 and 25 are used as a guide in decision-making, the designer should expect the MSD estimates to be much closer to the "correct" FE solution. The designer must, of course, decide in which situations MSD predictions alone can be accepted and when the FE solution must be obtained as well.

Two significant uncertainties will hamper the decision that the designer must make regarding the limit to be placed on

Fig. 25. Comparison of crest displacements between FE calculations and MSD predictions for different stress–strain curves (K_0 = 1.0): (*a*) H/D = 0.25, (*b*) H/D = 0.40, (*c*) H/D = 0.50.

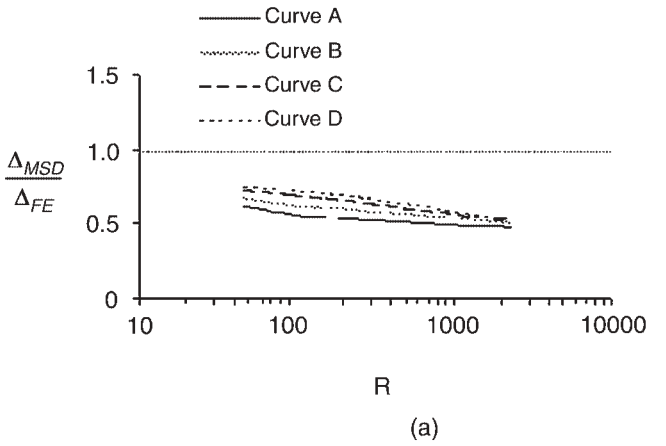

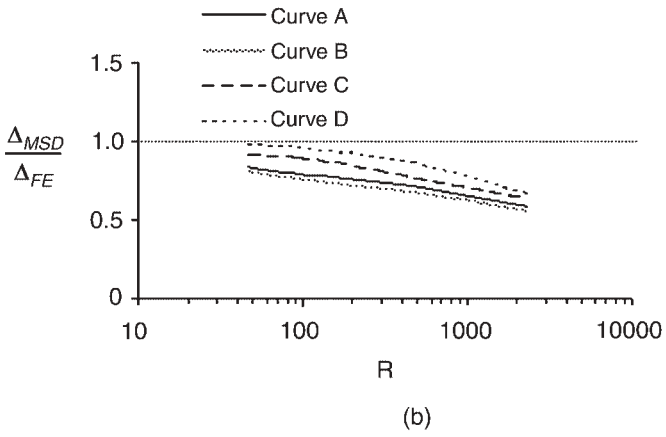

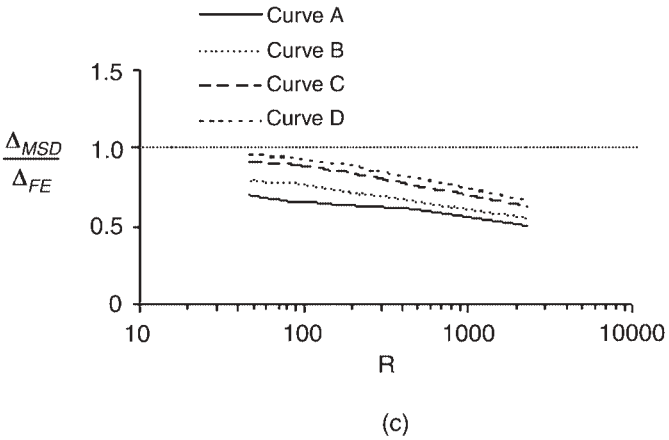

wall movement or soil strain. Designers should first realise that criteria for limiting strains to prevent damage in different classes of structure are rather approximate (Burland and Wroth 1974). The actual condition of the existing building or services that are partly located in the zone of influence of a new excavation will also be open to doubt. These inevitable uncertainties may lead the designer to the conclusion that even a factor 2 error in the MSD calculations can be tolerated.

Conclusions

Serviceability and safety requirements should be based on the fundamental understanding of the stress–strain behaviour of the soil. The design strength that limits the deformations should be selected according to the actual stress–strain data from each site, and not derived using arbitrary factors. The present study relates to the undrained soil response to excavation behind a cantilever retaining wall.

A new application of plasticity theory that combines statically admissible stress fields and kinematically admissible deformation mechanisms with distributed plastic strains can provide a unified solution for design problems. This application is different from the conventional applications of plasticity theory because it can approximately satisfy both safety and serviceability requirements by predicting stresses and displacements under working conditions. Also, it provides simple hand calculations for nonlinear soil behaviour which can give reasonable results compared with those from complex finite element analyses.

Displacements in the MSD method are controlled by the average soil stiffness in the zone of deformation. Stress–strain data from an undisturbed soil sample taken at the mid-height of the retaining wall prior to excavation can be used to deduce the average shear strength that can be mobilized at the required shear strain in MSD calculations.

More generalized statically admissible stress fields were derived for the MSD method to incorporate the K_0 effect. Although the MSD method overestimates the depth of tension cracks developed in soils and ignores wall friction, it gives lateral stress distributions similar to those calculated by FE analysis. Bending moments are very sensitive even to small changes in stress distribution, however, and care needs to be taken in selecting appropriate values.

Curves showing the variation in the ratios of crest deformations predicted by the MSD method compared with those calculated using FE analysis are plotted against Rowe's relative soil–structure stiffness for various in situ values of K_0, various stress–strain curves, and various excavation ratios. These curves can be useful in the preliminary design of retaining walls. They show that the MSD method underpredicts displacements, but generally by a factor smaller than 2, which could be acceptable in many practical design situations. Recalibration of MSD predictions based on the given curves could lead to even more accurate predictions.

The key advantage of the MSD method is that it gives the designers the opportunity to consider the sensitivity of a design proposal to the nonlinear behaviour of a representative soil element. It accentuates the importance of acquiring reasonably undisturbed samples and of testing them with an appropriate degree of accuracy in the local measurement of strains (e.g., 0.01%). The extra step of actually performing FE analyses remains open, with the advantage that the engineer would then have an independent check on the answer to be expected, within a factor of 2 on displacement and a factor of 1.5 on bending moment.

It has been illustrated that a wall designed to resist MSD earth pressure cannot collapse if the wall is designed to be ductile. If extra bending moments are induced due to excessive wall stiffness, plastic yielding will eliminate them as the wall displacement increases by a negligible amount.

Acknowledgements

The authors would like to thank Dr. Arul Britto for his advice and helpful comments. The authors are grateful to Cambridge Commonwealth Trust and Overseas Research Scheme for their provision of financial support to the first author.

References

Atkinson, J.H., Richardson, D., and Stallebrass, S.E. 1990. Effect of recent stress history on the stiffness of overconsolidated soil. Géotechnique, **40**(4): 531–540.

Bolton, M.D. 1993. Codes, standard and design guides. *In* Retaining structures. *Edited by* C.R.I. Clayton. Thomas Telford, London, UK. pp. 387–402.

Bolton, M.D., and Powrie, W. 1987. The collapse of diaphram walls retaining clay. Géotechnique, **37**(3): 335–353.

Bolton, M.D., and Powrie, W. 1988. Behaviour of diaphram walls in clay prior to collapse. Géotechnique, **38**(2): 167–189.

Bolton, M.D., and Sun, H.W. 1991. Modelling of bridge abutments on stiff clay. *In* Proceedings of the 10th European Conference on Soil Mechanics, Florence, Italy, 26–30 May 1991. A.A. Balkema, Rotterdam, The Netherlands. Vol. 1, pp. 51–55.

Bolton, M.D., Powrie, W., and Symons, I.F. 1989. The design of stiff in-situ walls retaining overconsolidated clay, part 1. Ground Engineering, **22**(8): 44–48.

Bolton, M.D., Powrie,W., and Symons, I.F. 1990*a*. The design of stiff in-situ walls retaining overconsolidated clay, part 1, short term behaviour. Ground Engineering, **23**(1): 34–39.

Bolton, M.D., Powrie, W., and Symons, I.F. 1990*b*. The design of stiff in-situ walls retaining overconsolidated clay, part II, long term behaviour. Ground Engineering, **23**(2): 22–28.

Bolton, M.D., Dasari, G.R., and Britto, A.M. 1994. Putting small strain non-linearity into Modified Cam Clay model. *In* Proceedings of the 8th International Conference on Computer Methods and Advances in Geomechanics (IACMAG), Morgantown, W. Va., 22–28 May 1994. *Edited by* J. Siriwardane and M.M. Zaman. A.A. Balkema, Rotterdam, The Netherlands. pp. 537–542.

British Standards Institution. 1994. Code of practice for earth retaining structures. BS 8002. British Standards Institution, London, UK.

Burland, J.B., and Wroth, C.P. 1974. Allowable and differential settlements of structures, including damage and soil–structure interaction. *In* Settlement of Structures, Proceedings of the Conference of the British Geotechnical Society, Cambridge. Pentech Press, London, UK. pp. 611–764.

Burland, J.B., Potts, D.M., and Walsh, N.M. 1981. Overall stability of free and propped embedded cantilever retaining walls. Ground Engineering, **14**(5): 28–32, 35–37.

Carder, D.R., and Symons, I.F. 1989. Long-term performance of an embedded cantilever retaining wall in stiff clay. Géotechnique, **39**(1): 55–75.

Dasari, G.R. 1996. Modelling the variation of soil stiffness during sequential construction. Ph.D. dissertation, Cambridge University, Cambridge, UK.

Dasari, G.R., and Britto, A.M. 1995. Strain-dependent Modified Cam Clay model. Technical Report CUED-SOILS/TR276, Cambridge University Engineering Department, Cambridge University, Cambridge, UK.

De Moor, E.K. 1994. Analysis of bored pile/diaphragm wall installation effects. Géotechnique, **44**(2): 341–347.

ECS. 1997. Eurocode EC7: geotechnical design. European Committee for Standardization (ECS), Brussels, Belgium.

Garrett, C., and Barnes, S.J. 1984. Design and performance of the Dunton Green retaining wall. Géotechnique, **34**(4): 533–548.

Hubbard, H.W., Potts, D.M., Miller, D., and Burland, J.B. 1984. Design of the retaining walls for the M25 cut and cover tunnel at Bell Common. Géotechnique, **34**(4): 495–512.

Jardine, R.J., Symes, M.J., and Burland, J.B. 1984. The measurement of soil stiffness in the triaxial apparatus. Géotechnique, **34**(3): 323–340.

Long, M. 2001. Database for retaining wall and ground movements due to deep excavations. Journal of Geotechnical and Geoenvironmental Engineering, ASCE, **127**(3): 203–224.

Masing, G. 1926. Eigenspannungen und Verfestigung beim Messing. *In* Proceedings of the 2nd International Congress of Applied Mechanics, Zurich, Switzerland. pp. 332–335.

Milligan, G.W.E., and Bransby, P.L. 1976. Combined active and passive rotational failure of a retaining wall in sand. Géotechnique, **26**(3): 473–494.

Osman, A.S. 2002. Mobilizable soil strength for geotechnical design of retaining walls. M.Phil. dissertation, Department of Engineering, Cambridge University, Cambridge, UK.

Padfield, C.J., and Mair, R.J. 1984. Design of retaining walls embedded in stiff clay. Construction Industry Research and Information Association, CIRIA Report R104.

Potts, D.M., and Fourie, A.B. 1985. The effect of wall stiffness on the behaviour of a propped retaining wall. Géotechnique, **35**(3): 347–352.

Powrie, W. 1985. Discussion on performance of propped and cantilevered rigid walls. Géotechnique, **35**(4): 546–548.

Powrie, W. 1996. Limit equilibrium analysis of embedded retaining walls. Géotechnique, **46**(4): 709–723.

Powrie, W., and Li, E.S.F. 1991. Finite element analyses of an in situ wall propped at formation level. Géotechnique, **41**(4): 499–514.

Powrie, W., Pantelidou, H., and Stallebrass, S.E. 1998. Soil stiffness in stress paths relevant to diaphragm walls in clay. Géotechnique, **48**(4): 483–494.

Puller, M., and Lee, T. 1996. Comparison between the design methods for earth retaining structures recommended by BS 8002:1994 and previously used methods. Proceedings of the Institution of Civil Engineers, Geotechnical Engineering, **119**(1): 29–34.

Roscoe, K.H., and Burland, J.B. 1968. On the generalized stress–strain behaviour of wet clay. *In* Engineering plasticity. *Edited by* J. Heyman and F.A. Leckie. Cambridge University Press, Cambridge, UK. pp. 535–609.

Rowe, P.W. 1955. Sheet pile walls encastre at the anchorage. Proceedings of the Institution of Civil Engineers, London, Part 1, Vol. 4.

Simpson, B., and Driscoll, R. 1998. Eurocode 7: a commentary. Construction Research Communications, Watford, UK.

Symons, I.F. 1983. Assessing the stability of a propped, in situ retaining wall in overconsolidated clay. Proceedings of the Institution of Civil Engineers, Part 2: Research and Theory, **75**: 617–633.

Symons, I.F., and Carder, D.R. 1992. Field measurement on embedded retaining walls. Géotechnique, **42**(1): 117–126.

Tedd, P., Chard, B.M., Charles, J.A., and Symons, I.F. 1984. Behaviour of a propped embedded retaining wall in stiff clay at Bell Common Tunnel. Géotechnique, **34**(4): 513–532.